Mon. Not. R. astr. Soc. (1992) **258,** 177–188

Properties of cooling flows in a flux-limited sample of clusters of galaxies

A. C. Edge,[1] G. C. Stewart[2] and A. C. Fabian[1]
[1]*Institute of Astronomy, Madingley Road, Cambridge CB3 0HA*
[2]*X-ray Astronomy Group, University of Leicester, Leicester LE1 7RH*

Accepted 1992 March 5. Received 1992 January 21; in original form 1991 October 8

SUMMARY

We present an analysis of the mass flow rates of cooling flows in an X-ray flux-limited sample of clusters of galaxies, in which most of the clusters have been observed with both imaging and spectroscopic detectors. Using high-quality images and constraints from broad-band spectra, we find that the fraction of clusters with central cooling times less than the Hubble time is high (at least 70 per cent and possibly 90 per cent), indicating that cooling flows are a common and long-lived phenomenon. The fraction is higher than found in previous studies, due to our consideration of the effects of the spatial resolution and the signal-to-noise ratio of the images. We also determine the fraction of cooling flows with optical line emission and the space density of clusters as a function of the mass flow rate. The clusters that are not cooling flows are apparently recent mergers (e.g. A2256) and contain radio halo sources. We investigate the impact of cluster evolution through mergers on the evolution of the mass flow rate in four well-studied cooling flows, and estimate the length of time for which they have been undisturbed.

Key words: galaxies: clustering – cooling flows – X-rays: galaxies.

1 INTRODUCTION

The most prominent feature of the X-ray images of most clusters of galaxies is a strong peak around the brightest galaxy (often a cD) at the centre of the cluster. The cooling time of the central gas is usually inferred to be less than the age of the cluster, assumed to be similar to the age of the Universe. The cooling of the gas there leads to an inward flow which is required to maintain pressure equilibrium, i.e. a 'cooling flow' forms (see Fabian, Nulsen & Canizares 1991 for a recent review).

Clusters of galaxies have recently been found from X-ray studies to be evolving rapidly (Edge *et al.* 1990; Gioia *et al.* 1990a), most probably through hierarchical mergers. This result provides a coherent framework for the interpretation of other observations of clusters and superclusters where substructure in galaxy counts, velocity distribution and X-ray emission is common. The structure of a cooling flow can be disrupted by the merger of two similar clusters (McGlynn & Fabian 1984), so cooling flows may provide a powerful tool to study the effect of mergers on cluster structure. The fraction of clusters with cooling flows should be related to the frequency at which disruptive mergers occur and the rate at which the gas in the core re-establishes itself close to an equilibrium state.

Cooling flows in nearby clusters are known to be common (Stewart *et al.* 1984; Arnaud 1988). These authors used data from the *Einstein Observatory* Imaging Proportional Counter (IPC) and High Resolution Imager (HRI), where the selection of clusters observed was essentially arbitrary and included many clusters of low X-ray luminosity and moderately high redshift ($z > 0.1$).

In two companion papers (Lahav *et al.* 1989; Edge *et al.* 1990), a flux-limited sample of clusters was compiled and combined with data from the *Einstein Observatory* and *EXOSAT* to include the most accurate fluxes and temperatures. Here we have used the imaging data available for all but four of this sample to determine the distribution of cooling flow rates and investigate the frequency of cooling flows in a complete sample. We have carefully considered the effect of spatial resolution on the determination of the central cooling time, which is a strong function of radius.

2 THE SAMPLE

Details of the *EXOSAT* observations are given in Edge & Stewart (1991a), while those for the *Einstein Observatory* observations can be found in Stewart *et al.* (1984) and Arnaud (1988). These authors deprojected the X-ray surface brightness profiles of the clusters to find gas density, temper-

ature and mass flow rate profiles using the procedure of Fabian *et al.* (1981). There are four clusters which are not in the original Arnaud list or the *EXOSAT* sample, namely A1367, A1736, A3391 and A3552, which we have deprojected using the same method. Hydrostatic equilibrium is assumed by the procedure and this requires some knowledge of the gravitational potential distribution of the cluster. The potential is usually determined from the cluster velocity dispersion, which is often poorly measured. In particular, high values of the velocity dispersion are suspect when the X-ray luminosity is low, and are probably due to contamination by outlying galaxies, or to substructure. We have therefore reanalysed all the clusters in the Arnaud sample where high velocity dispersions (>1250 km s^{-1}) were used to determine the gravitational potential in the deprojection analysis. The effect of such high, optically determined values is to overestimate the central pressure and the cooling time, and hence underestimate the mass flow rate, $\dot{M}$. Instead of the high values of velocity dispersion, we used values consistent with the measured X-ray temperature (Edge & Stewart 1991b). We have also reanalysed four clusters observed with high signal-to-noise ratios in order to examine the cooling flows in them in detail (see Section 4.3).

We define a cooling flow as occurring when the central cooling time of a cluster is found to be less than the assumed age of the cluster (the Hubble time or less). The mass flowing in through a shell at radius r, $\dot{M}(<r)$, is that required to maintain the pressure balance as the gas cools. It is deposited within that radius (see Fabian *et al.* 1985). The integrated mass flow rates quoted in this paper are the mass inflow rates within the radius at which the cooling time equals the Hubble time (the cooling radius, r_c).

We constrained the allowed temperature profile of the cluster gas outside the cooling radius with the mean cluster gas temperature determined from high-quality X-ray spectra obtained from broad-beam instruments. Errors for the derived quantities were estimated from a Monte Carlo method in which the observed counts in the X-ray surface brightness profiles are perturbed by amounts appropriate to the photon noise. The new profiles are then deprojected and values of $\dot{M}$ produced. The process was repeated 100 times and the values of $\dot{M}$ accumulated in ascending order. The central values quoted in Table 1 are the 50th percentile; we also give the 10th and 90th percentiles as estimates of the uncertainty on $\dot{M}$.

An important issue addressed here is the effect of the spatial resolution of the images, since, for clusters where the resolution is of the order of the cooling radius (~ 200 kpc), the central cooling time is overestimated and a cooling flow missed. The observed clusters cover a wide range of redshift ($z=0$–0.18) and the instrumental resolution for many observations was ~ 1 arcmin (in particular for the IPC), comparable to the size of the cooling region in the more distant clusters ($z>0.05$).

The analysis in this paper assumes a single-phase intracluster medium (ICM), i.e. there is only one temperature of gas at any given radius. Given the complex nature of the ICM with many phases in pressure equilibrium, this is an oversimplification. However, a detailed multiphase analysis of several well-studied clusters by Thomas, Fabian & Nulsen (1987) has shown that the results of the multiphase method are similar to those from the single phase.

Recent analysis of the *Einstein Observatory* Solid State Spectrometer (SSS) spectra of clusters by White *et al.* (1991) has revealed an excess column density in the cores of cooling flows. As discussed by Johnstone *et al.* (1992), the effect of any excess column density is to increase the measured mass flow rate. We have not used any excess column densities in our analysis, so our results probably underestimate the total mass flow rates.

We assume throughout a Hubble constant, H_0, of 50 km s^{-1} Mpc^{-1}. In order to be consistent with the work of Arnaud (1988), we adopt a Hubble time of 2×10^{10} yr throughout (i.e. q_0 of 0.0). We show below that if a lower Hubble time is used it does not affect the classification of a cluster as a cooling flow *when the effect of resolution is considered.*

The sample used here is consistent with the other large X-ray selected sample of clusters, the *Einstein* Medium Sensitivity Survey, EMSS (Gioia *et al.* 1990b), in terms of the X-ray luminosity function and source counts. This implies that there are no serious selection effects between the two samples.

3 RESULTS

The results of the analysis are summarized in Table 1 which gives the redshift, 2–10 keV flux, 2–10 keV luminosity, the central cooling time, the radial bin size used in the analysis and the mass flow rate at the radius at which the cooling time is less than 2×10^{10} yr (the cooling radius) for the 51 clusters in the sample with images, of which nine are at low galactic latitude ($|b|<20°$).

Fig. 1 shows the mass flow rate plotted against the 2–10 keV cluster luminosity. There is clearly a large scatter in mass flow rate with cluster luminosity, but a general trend for

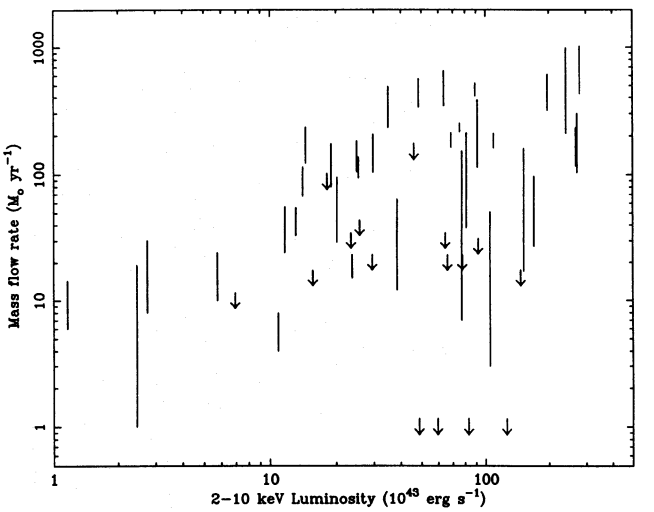

Figure 1. Mass flow rate plotted against 2–10 keV luminosity. The upper limits are clusters where the 10 percentile is zero. Clusters that are definitely not cooling are given arbitrary upper limits of 1 $M_\odot$ yr^{-1}. The upper envelope of the distribution of $\dot{M}$ is consistent with a maximum of ~ 40 per cent of the total bolometric luminosity of the cluster coming from the cooling flow. The clusters nearest this limit (Hydra-A and MKW3s) are both cool, poor clusters. The more typical cooling flow is at most 20 per cent of the total bolometric luminosity.

Table 1. The flux-limited sample of clusters. Column 2 contains the redshift and a note as to whether emission lines have been detected from the brightest galaxy; a tick for yes, a cross for no and a bar for unknown. Column 3 gives the flux and the instrument used to determine it; 1 for *EXOSAT*, 2 for the *Einstein Observatory* MPC and 3 for *HEAO-1* A-2. Column 5 gives the central cooling time with 1σ error. Column 6 gives the bin size used in the analysis and the imaging detector used; L for *EXOSAT* LE, I and H for the *Einstein Observatory* IPC and HRI respectively. Column 7 gives the 10, 50 and 90 percentiles for the integrated mass flow rate for a critical cooling time of 2×10^{10} yr. The cases with asterisks are definitely not cooling. This table is a revised version of the one in Edge *et al.* (1990) when Coma was left uncorrected for flux lost in the collimator.

Cluster	Redshift	2-10 keV Flux (10^{-11} erg cm^{-2} s^{-1})	2-10 keV Luminosity (h_{50}^{-2} erg s^{-1})	Central Cooling Time (10^9 yr)	Bin Size (kpc)	Mass Flow Rate ($M_\odot$ yr^{-1})
A426*	0.0183 ✓	75.0 [1]	1.10×10^{45}	0.48±0.02	31 I	161,183,208
Ophiuchus*	0.028 —	44.5 [1]	1.52×10^{45}	3.1±7.4	29 L	17,75,159
Coma	0.0232 ×	32.0 [1]	7.50×10^{44}	95±239	47 I	0*
Virgo	18 Mpc ✓	30.0 [1]	1.16×10^{43}	0.03±0.01	3 L	6,10,13
A2319*	0.0564 ×	12.1 [2]	1.70×10^{45}	13.1±2.2	73 I	27,66,97
A3571	0.0391 —	11.5 [1]	7.67×10^{44}	7.8±12.9	35 L	7,79,150
Centaurus	0.0109 ✓	11.2 [1]	5.75×10^{43}	0.49±0.10	10 L	10,18,25
Tri. Aust.*	0.051 —	11.0 [1]	1.26×10^{45}	65±254	160 L	0
3C129*	0.022 —	9.59 [1]	2.02×10^{44}	5.1±4.5	44 L	28,61,95
AWM7*	0.0172 ×	9.14 [1]	1.17×10^{44}	3.9±1.2	65 I	23,42,56
A754	0.0528 ×	8.53 [1]	1.05×10^{45}	9.5±12.5	48 L	3,24,52
A2029	0.0767 ×	7.52 [2]	1.97×10^{45}	3.8±0.7	99 I	344,402,449
A2142	0.0899 ×	7.50 [1]	2.72×10^{45}	3.0±0.8	48 H	105,188,300
A2199	0.0309 ✓	7.12 [1]	2.97×10^{44}	2.4±1.8	42 L	103,150,204
A3667	0.0530 ×	6.68 [2]	8.28×10^{44}	165±236	112 I	0*
A478	0.0882 ×	6.63 [1]	2.41×10^{45}	2.3±0.5	70 L	210,570,990
A85	0.0518 ✓	6.37 [2]	7.54×10^{44}	3.8±0.6	69 I	215,236,252
A3266	0.0594 ×	5.90 [2]	9.21×10^{44}	21.5±17.3	70 H	0,10,27
A401	0.0748 ×	5.88 [2]	1.47×10^{45}	20.1±5.9	92 I	0,12,15
0745-19*	0.1028 ✓	5.87 [1]	2.80×10^{45}	2.1±0.5	32 L	430,702,1020
A496	0.0320 ✓	5.67 [1]	2.54×10^{44}	2.1±0.3	43 I	93,112,136
A1795	0.0616 ✓	5.30 [1]	8.91×10^{44}	2.5±0.4	81 I	412,478,523
A2256	0.0601 ×	5.20 [2]	8.32×10^{44}	175±38	153 I	0*
Cygnus-A*	0.057 ✓	4.78 [1]	6.87×10^{44}	4.2±0.5	92 I	162,187,210
0336+09	0.0349 ✓	4.67 [1]	2.49×10^{44}	0.90±0.11	35 L	105,142,181
A1060	0.0114 ✓	4.36 [1]	2.45×10^{43}	2.2±3.3	16 L	2,9,19
A3558	0.0478 ×	4.21 [1]	4.23×10^{44}	–	–	–
A644*	0.0704 ×	4.15 [2]	9.15×10^{44}	8.7±1.1	146 I	114,326,382
A1651	0.0825 ×	3.67 [3]	1.12×10^{45}	–	–	–
A3562	0.0499 ×	3.52 [1]	3.86×10^{44}	4.5±4.8	25 L	12,45,65
A1367	0.0215 ×	3.45 [1]	6.93×10^{43}	21.5±3.7	92 I	0
A399	0.0715 ×	3.41 [2]	7.76×10^{44}	25.4±5.0	139 I	0
A2147	0.0356 —	3.28 [1]	1.82×10^{44}	15.2±24.5	83 L	0,54,88
A119	0.0440 ×	3.03 [1]	2.58×10^{44}	14.6±9.3	86 L	0,23,38
A3158	0.0590 ×	2.99 [2]	4.61×10^{44}	23.2±3.8	197 I	0
Hydra-A	0.0522 ✓	2.90 [2]	3.49×10^{44}	1.8±0.7	50 L	233,315,489
A2065	0.0721 —	2.79 [2]	6.46×10^{44}	33.3±8.2	136 I	0
A2052	0.0348 ✓	2.66 [1]	1.41×10^{44}	1.1±0.2	40 L	68,90,114
A2063	0.0337 ×	2.64 [2]	1.31×10^{44}	4.1±1.0	68 I	33,45,55
A1644	0.0456 ×	2.60 [2]	2.38×10^{44}	13.5±4.6	59 I	15,19,23
Klemola44	0.0283 —	2.55 [2]	8.91×10^{43}	–	–	–
A262	0.0164 ✓	2.35 [1]	2.74×10^{43}	0.87±0.40	23 I	26,47,67
A2204	0.1523 —	2.20 [3]	2.35×10^{45}	–	–	–
A2597	0.0824 ✓	2.09 [2]	6.35×10^{44}	11.1±2.0	185 I	343,480,653
A1650	0.0845 —	2.07 [2]	6.62×10^{44}	54±103	160 I	0
A3112	0.0746 ×	1.95 [1]	4.84×10^{44}	2.1±1.0	82 L	335,430,565
A3532	0.0585 —	1.95 [2]	2.95×10^{44}	44.1±14.9	141 I	0
A4059	0.0478 ✓	1.88 [1]	1.89×10^{44}	3.5±8.5	35 L	80,124,173
A3391	0.0545 ×	1.79 [2]	2.35×10^{44}	31.8±5.7	140 I	0
MKW3s	0.043 ✓	1.79 [2]	1.45×10^{44}	4.0±0.9	77 I	122,151,188
A1689	0.181 ×	1.75 [2]	2.68×10^{45}	13.8±2.3	190 I	117,164,234
A576	0.0381 ×	1.72 [1]	1.09×10^{44}	15.1±3.3	77 I	4,6,8
A2244	0.1024 —	1.71 [2]	8.09×10^{44}	12.2±2.0	120 I	37,82,210
A2255	0.0798 ×	1.71 [2]	4.87×10^{44}	143±268	97 I	0*
A1736	0.046 ×	1.70 [2]	1.58×10^{44}	32.9±7.5	115 I	0

Table 2. The distribution of mass flow rates in five luminosity classes.

L_x	10^{43}–3×10^{43} (erg s^{-1})	3×10^{43}–10^{44} (erg s^{-1})	10^{44}–3×10^{44} (erg s^{-1})	3×10^{44}–10^{45} (erg s^{-1})	10^{45}–3×10^{45} (erg s^{-1})
Cooling	3	1	13	11	10
Non-cooling	0	0	0	4	0
Unresolved	0	1	3	4	1
Percentage	100	50(100)	81(100)	58(79)	91(100)
Average $\dot{M}$ ($M_\odot$ yr^{-1})	12	18	78	242	250

more massive flows in the more luminous clusters. The distribution of cooling flow rates with luminosity can be seen in Table 2 where the clusters have been subdivided into five luminosity bins. The lowest fraction of cooling flows is found in the moderate-luminosity bin ($L_x = 10^{44.5\text{-}45}$ erg s^{-1}). This bin contains two of the three Rood–Sastry B, binary clusters in the sample (Coma and A2256) and other clusters with two dominant galaxies (A2255 and A3667). We shall return to this point in Section 4.1.

70 per cent of all the clusters in the sample and 67 per cent of all high galactic latitude clusters have directly measured central cooling times less than the Hubble time. This is higher than found in arbitrarily selected samples (Stewart *et al.* 1984; Arnaud 1988).

The distribution of cooling times in Fig. 2 shows that, even if a much lower critical time is used (e.g. 5×10^9 yr), then a large fraction (42 per cent) of clusters can still be defined as cooling flows by the simple definition. As we will show in the next section, the use of central cooling times is highly resolution dependent and it is not possible to assign to any cluster a definite 'cooling time' as this quantity decreases rapidly in the core. So Fig. 2 and the fraction of cooling flows are strongly affected by the resolution of the data. The distribution of mass flow rates in Fig. 3 indicates that the majority of the clusters have $\dot{M} < 100\ M_\odot$ yr^{-1} but a tail to 600 $M_\odot$ yr^{-1} exists.

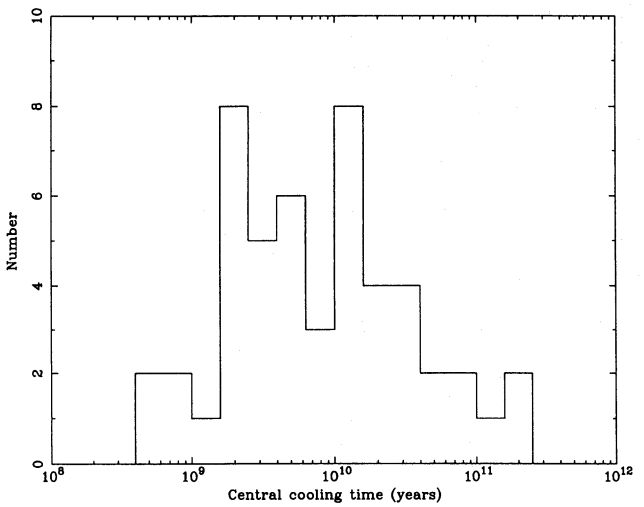

Figure 2. Histogram of the central cooling times in the whole sample.

3.1 The effect of spatial resolution

The most important factor affecting the analysis of the sample is the spatial resolution of the original data. The analysis is performed on surface brightness profiles of fixed annular bin size, chosen to give the best resolution and signal in the central and outer bins. The inferred cooling time is strongly dependent on radius, so quoting central cooling times is as 'arbitrary' as quoting central gas densities. Therefore basing the definition of a cluster as a cooling flow on *only* a central cooling time leads to confusion where that value is just above or below the assumed age or where the resolution is poor. To avoid these pitfalls we have investigated the effects of resolution on clusters where we have more than one image (and resolution), and then how resolution affects those clusters which appear not to be cooling flows.

To demonstrate the effect of improved resolution for individual clusters we plot in Fig. 4 the central cooling time against bin size in kiloparsecs for sets of clusters which were observed with the *Einstein Observatory* IPC and HRI or *EXOSAT* LE (or all three). There are a number of important features in this plot. The first is that as the resolution is increased (i.e. using HRI instead of IPC data), the cooling time always decreases. Secondly, clusters with similar mass flow rates lie along lines of $t_c \propto r^{1.5}$, where r is the bin size, as expected from roughly similar, constant (within a factor of 3) pressures inside the cooling radius. Clusters with higher central pressures have higher mass flow rates. These two points allow us to consider cases where the measured central cooling time is greater than the Hubble time and estimate whether it could be a cooling flow if data with better resolution were available. Fig. 5 shows central cooling time plotted against the bin size in kiloparsecs for the whole sample.

For clusters with measured central cooling times greater than the Hubble time (open circles), ten lie between 2×10^{10} and 5×10^{10} yr. Given the strong trend for cooling time and resolution seen in Fig. 4 it can be expected that most, if not all, of these clusters would have a central cooling time less than the Hubble time if data with better resolution were available.

This can be thought of in a different way. As the resolution is related primarily to the redshift (see Fig. 6), clusters with resolutions greater than 100 kpc are simply at larger redshift. A moderate (10–100 $M_\odot$ yr^{-1}) cooling flow is resolvable at 100-kpc resolution but when its redshift is above 0.05 (equivalent to 1-arcmin resolution) the cooling core is no

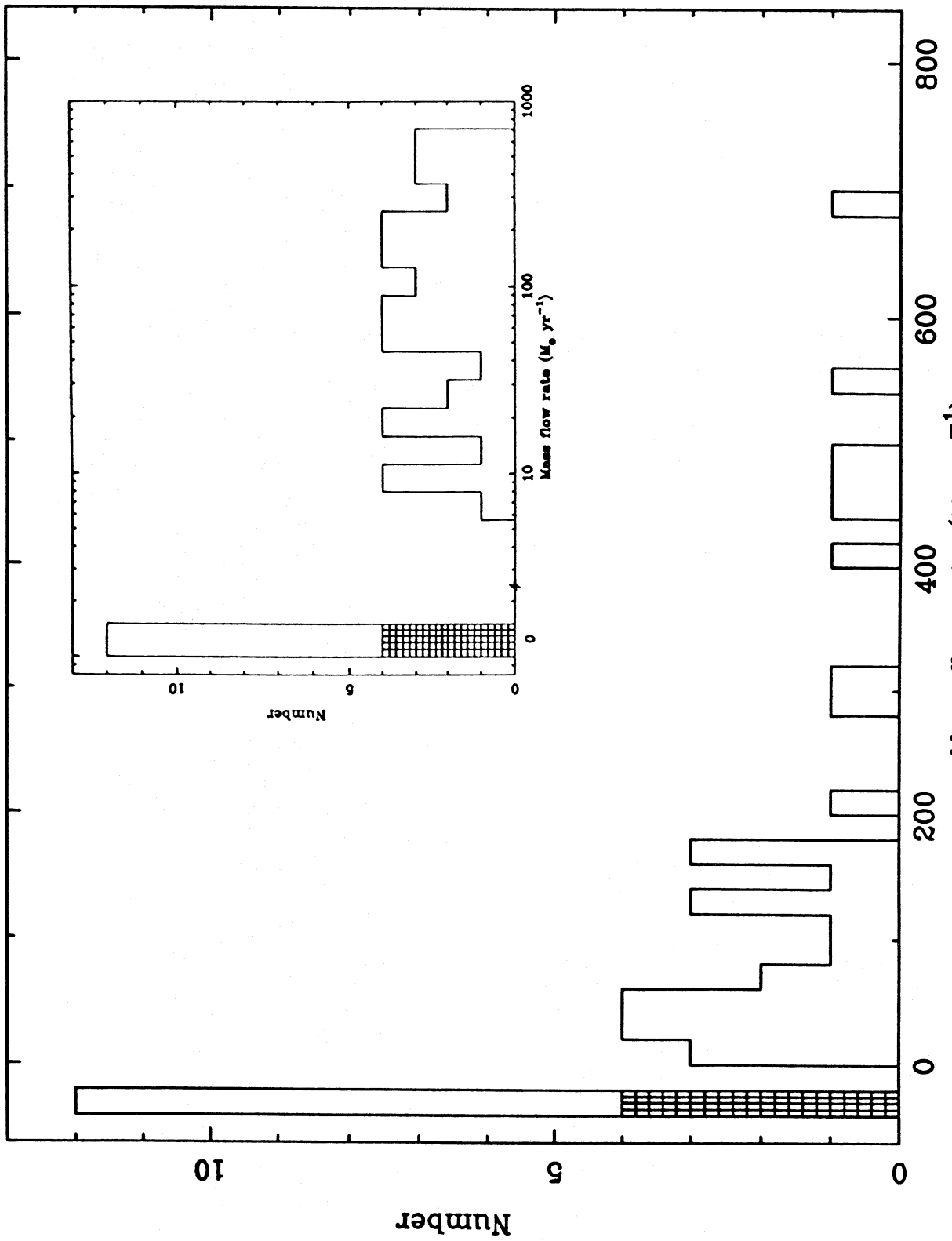

Figure 3. Histogram of the mass flow rates in the whole sample. The non-cooling-flow clusters are shown with negative or zero mass flow rate. The inset figure shows the distribution in logarithmic bins.

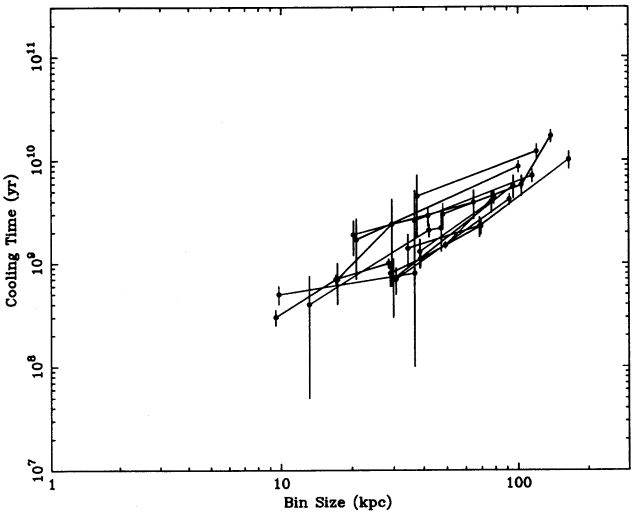

Figure 4. Central cooling time against bin size for clusters where we have the *Einstein Observatory* IPC and HRI or *EXOSAT* LE data. The solid lines join the points for each cluster.

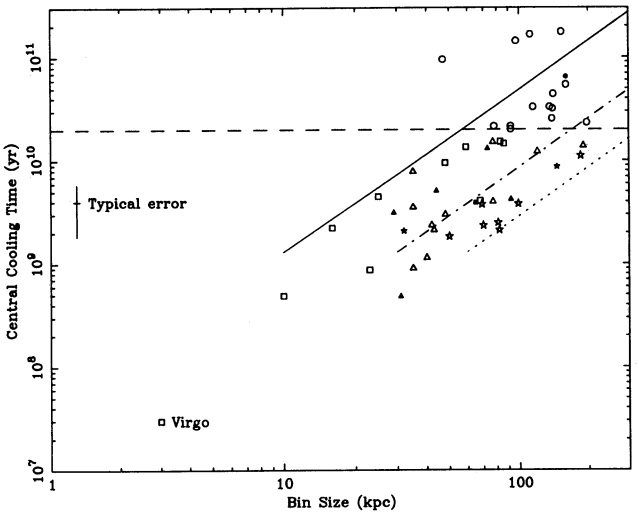

Figure 5. Central cooling time against bin size for the whole sample. The symbols mark clusters of different mass flow rates: squares, $\dot{M} < 50\ M_\odot\ \mathrm{yr}^{-1}$; triangles, $\dot{M} = 50$–$200\ M_\odot\ \mathrm{yr}^{-1}$; stars, $\dot{M} > 200\ M_\odot\ \mathrm{yr}^{-1}$; and circles, unknown. The filled symbols are the low galactic latitude clusters in the sample. The dashed line marks the Hubble time, 2×10^{10} yr. The diagonal lines mark the locus of clusters with the same measured mass flow rate (solid line marks $\dot{M} \approx 5\ M_\odot\ \mathrm{yr}^{-1}$, dot-dashed line marks $\dot{M} \approx 100\ M_\odot\ \mathrm{yr}^{-1}$ and dashed line marks $\dot{M} \approx 500\ M_\odot\ \mathrm{yr}^{-1}$). Each cluster is plotted once.

longer resolved. All but one of the clusters with resolution of greater than 100 kpc and central cooling times greater than 2×10^{10} yr are at a redshift exceeding 0.05. Since they are drawn from the same sample, these higher redshift clusters should have the same fraction of cooling flows and similar ratios of mass flow rates. Of the 36 clusters with resolution better than 100 kpc, 31 are definitely cooling flows and a further three are just above the critical time. Therefore the fraction of cooling flows is between 86 and 94 per cent. Applying these fractions to the 14 clusters at higher redshifts, we expect 12 or 13 cooling flows instead of the four found. Similarly, the higher resolution subsample has seven clusters with $\dot{M} > 200\ M_\odot\ \mathrm{yr}^{-1}$, 12 with $\dot{M}$ of 50–200 $M_\odot$

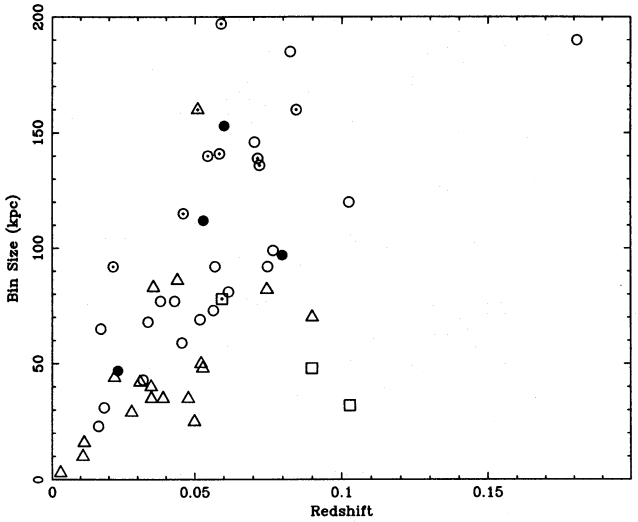

Figure 6. Bin size used in the deprojection analysis against redshift. IPC data points are circles, LE are triangles and HRI are squares. The filled circles mark clusters that are unlikely to be cooling flows and those marked with dots are possibly 'unresolved'. The majority of points lie in a cone that corresponds to a fixed angular size of 48 to 90 arcsec.

yr^{-1} and 11 with $\dot{M} < 50\ M_\odot\ \mathrm{yr}^{-1}$, whereas the lower resolution sample has two, two and zero, respectively. The cooling flows with lower mass rates are clearly missing from the lower resolution subsample. If the distribution of mass flow rates holds in this sample, then we can conclude that most of the clusters which have measured cooling times above the Hubble time *are* cooling flows with mass flow rates less than $100\ M_\odot\ \mathrm{yr}^{-1}$.

Therefore, from Fig. 5 we calculate a 'resolution-corrected' fraction for the high galactic latitude sample of about 90 per cent, *when the effect of different bin sizes is taken into account.*

There are four clusters with central cooling times almost an order of magnitude higher than the rest. Although the errors on these values are relatively large, these four clusters lie in a very different region from the other clusters in the plot. The best-studied case is Coma which is found to be marginally cooling if the X-ray centre is chosen to be the local X-ray peak on NGC 4874 (Edge & Stewart 1991a). The mass flow rate in this case is very small, considering the high luminosity of the cluster as a whole, so any focused cooling flow is unimportant compared to the cluster. This illustrates that, even in non-cooling-flow clusters, there is the possibility of localized cooling around the largest galaxies. [Also, Fabian, Nulsen & Canizares (1984) have pointed out that the Coma cluster may have an 'unfocused' cooling flow, in which no central galaxy dominates the potential and gas cools out over a large radius.]

Virgo (M87) stands out in Fig. 6 as we have very good spatial resolution for it (3 kpc). It appears not to fit on the 'correlation' between cooling time and resolution for its measured mass flow rate. This is due partly to the role of the central galaxy potential on scales less than 10 kpc and also to the fact that we plot bin size (i.e. the outer edge of the bin) and not the bin centre. These effects distort the straight-line fit. The effect is seen to a lesser extent in the next best

resolved point, Centaurus, which is a similar-size cooling flow.

As clusters are known to be evolving rapidly (Edge *et al.* 1990; Gioia *et al.* 1990a), many clusters have existed in their present form for a time significantly shorter than the Hubble time. This should result in smaller mass flow rates if $\dot{M} \propto r$ (however, see Section 4.3), but will not result in the redefinition of cooling flows as non-cooling flow clusters, since the central cooling time decreases steadily in the core for all mass flow rates (Fig. 4). The most important factor in determining whether a cluster is a cooling flow is the resolution of the X-ray image, not the assumption of the Hubble time. The high fraction of cooling flows is unrelated to our use of 2×10^{10} yr; if we had chosen 10^{10} yr the conclusion would be the same except that there would be more 'unresolved' cooling flows. Only when cluster ages of 2×10^{9} yr or less are considered would there be a question as to whether there is at least a small amount of gas in the core which has a shorter cooling time.

3.2 Is the high cooling-flow fraction related to sample selection?

The detection efficiency of clusters in imaging X-ray surveys depends strongly on whether or not the cluster is a cooling flow (Pesce *et al.* 1990). However, unlike surveys based on X-ray imaging data such as the EMSS, in which surface brightness effects dominate, our sample was selected on the basis of data from large field-of-view, 2–10 keV instruments. As cooling flows are observed to contribute at most 40 per cent of the total 2–10 keV flux of a cluster (Fig. 1), it would be difficult to contrive a scenario where cooling flows are heavily over-represented in this flux-limited sample. Also, as it has roughly equal numbers of clusters in each logarithmic luminosity bin, there is no strong bias for, or against, clusters with low luminosity ($\sim 3 \times 10^{43}$ erg s^{-1}) and low mass flow rates.

As an additional point, Pesce *et al.* (1990) note that for the EMSS to have detected as many clusters as it did, the fraction of cooling flows had to be high (> 70 per cent), as low surface brightness clusters such as Coma would have been difficult to detect using the source-finding algorithms used in the EMSS. Therefore a separate data set supports the high cooling-flow fraction found here.

3.3 Is this high cooling-flow fraction consistent with the work of Arnaud?

Before we can assert that the high fraction of cooling flows is a general property of clusters we must determine whether the result is consistent with other samples (i.e. Arnaud 1988). The sample of 107 clusters considered by Arnaud are almost all Abell clusters and were 'pseudo-randomly' selected by the *Einstein Observatory* observers over the lifetime of the satellite. To check the effects of resolution in that sample, we have plotted in Fig. 7 the cooling time against bin size for all the Arnaud clusters not in our sample, 72 in total, as in Fig. 6. There is clearly a much higher fraction of clusters with poor resolution (> 100 kpc) and hence much higher central cooling time. However, most of the points lie below the extrapolated line for low mass flow rate indicating that, with improved resolution (and signal), the majority of the clusters

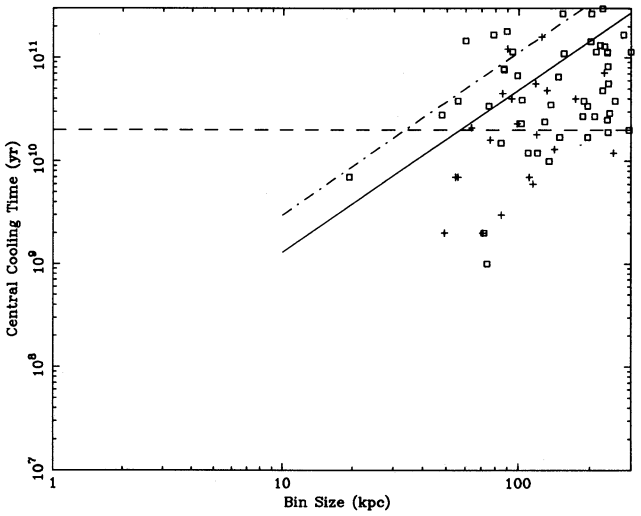

Figure 7. Central cooling time against bin size for the sample of Arnaud (1988). Note that the clusters in our sample are excluded. The squares mark clusters with assumed velocity dispersions greater than 1000 km s^{-1} and crosses those with dispersions less than 1000 km s^{-1}. The lines are as in Fig. 6 apart from the dot–dashed line which marks the line for the low-mass cooling-flow limit ($\dot{M} \approx 5\ M_{\odot}$ yr^{-1}) if an overestimated velocity dispersion is used.

would be found to be cooling flows. About 20 per cent of the Arnaud sample lie above the low mass flow rate line and are apparently not cooling flows. This fraction is somewhat larger than that found in our sample, but it should be noted that the central cooling time is sensitive to the effects of the assumed potential, especially the cluster velocity dispersion. In the Arnaud sample, 51 clusters have assumed velocity dispersion $\geqslant 1000$ km s^{-1}, as opposed to 21 < 1000 km s^{-1}, which is the inverse of the expected distribution (Zabludoff, Huchra & Geller 1990). These high velocity dispersions are likely to lead to central cooling times which are systematically overestimated. If the cooling times are corrected by a factor of 2 to compensate for the overestimated velocity dispersions (equivalent to decreasing the velocity dispersion to 700 km s^{-1}), then the fraction of non-cooling-flow clusters is 10 per cent. Therefore the relative fractions of cooling- and non-cooling-flow clusters in the Arnaud sample are similar to those in the brightest cluster sample, once the effects of resolution and assumed potential are taken into account. We conclude that the Arnaud sample is consistent with the high cooling-flow fraction found in the flux-limited sample presented here.

3.4 Space density

We have calculated a 'mass flow rate function' (analogous to the luminosity function) for the cooling flows. This is shown in Fig. 8. The space density of cooling flows with $\dot{M} > 100\ M_{\odot}$ yr^{-1} is 1×10^{-7} cluster Mpc^{-3}. This is a relatively crude estimate as the mass flow rate is only loosely related to the X-ray luminosity (Fig. 1), so the assumptions involved in the determination of the luminosity function about the detectability of a cluster in a flux-limited sample are weakened. However, the estimate should be good to at most a factor of 2 and is likely to be an underestimate since there are a

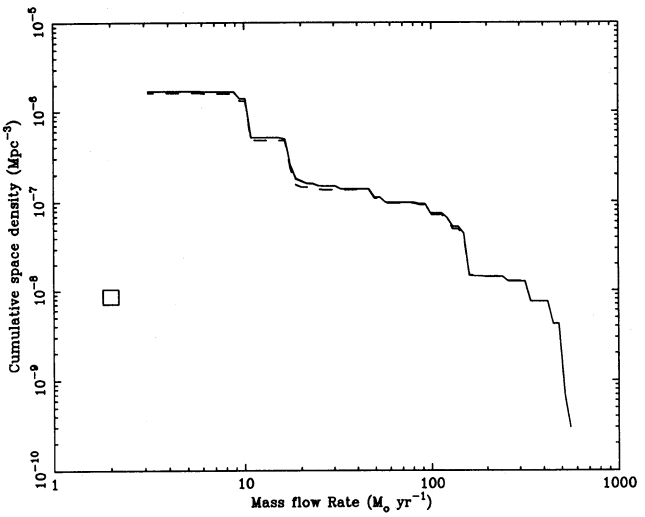

Figure 8. The cumulative mass flow rate function for all high galactic latitude clusters. The square marks the space density of all non-cooling-flow clusters. The two lines indicate the effect of the inclusion of the under-resolved cooling flows with estimated mass flow rates.

number of large cooling flows ($\dot{M} > 100\ M_\odot\ \mathrm{yr}^{-1}$) in clusters with relatively low luminosity ($< 10^{44.5}$ erg s^{-1}) which are less likely to be included in a flux-limited sample.

In addition to the space density of cooling flows, a space density of non-cooling-flow clusters can be calculated. Taking the four clusters which clearly do not contain cooling flows, we calculate a space density of 9×10^{-9} cluster Mpc^{-3} which is consistent with the space density of such hot, high-luminosity clusters.

From the space density of cooling flows, we can also calculate the mean space density of the mass flow rate. For this sample we estimate the volume-averaged deposition rate is $10^{-4}\ M_\odot\ \mathrm{yr}^{-1}\ \mathrm{Mpc}^{-3}$. This is about 1 per cent of the mean star formation rate in the present Universe from galaxies such as our own, assuming a space density for such galaxies of 10^{-2} Mpc^{-3} and a star formation rate per galaxy of 1 $M_\odot$ yr^{-1}. Over a Hubble time the mean cooling flow rate corresponds to $2 \times 10^{6}\ M_\odot$ Mpc^{-3} or approximately a factor of 200–400 less than the volume-averaged mass density of field galaxies (Efstathiou, Ellis & Peterson 1988), assuming a mass-to-light ratio of 4–8. Therefore, present-day cooling flows can account for the formation of only a relatively small fraction of all galaxies. However, in cluster cores where the mass deposition is concentrated, the total deposited mass is a large fraction of the inferred mass.

3.5 Optical line emission

Many central galaxies in cooling flows exhibit strong optical line emission (Cowie *et al.* 1983; Hu, Cowie & Wang 1985; Johnstone, Fabian & Nulsen 1987; Heckman *et al.* 1989), mainly Hα+[N II] and [O II], which has been used to infer that certain clusters are cooling flows, purely from optical data (Donahue, Stocke & Gioia 1992). The luminosity of the Hα line is several orders of magnitude larger than can be accounted for if the cooling hydrogen recombines once (Johnstone *et al.* 1987). There are also cooling flows that show no detectable line emission (but are consistent with single hydrogen recombination), most notably A2029. Therefore the lack of a detectable line does not exclude the cooling of gas through recombination at levels consistent with the measured mass deposition rate.

In order to investigate the relationship between optical line emission and the presence of a cooling flow, we have searched the literature and found those cases where line emission has been detected (denoted by a tick in Table 1). We could find no optical spectrum for 11 clusters. Of the 44 with some optical information, 17 have some line emission. This is very much a lower limit, given the range in line strength in clusters and the varied quality of spectra in the literature. However, it should be a reasonable estimate of the fraction of clusters showing moderate line emission, i.e. $\sim 5 \times 10^{40}$ erg s^{-1} in Hα (the detection limit for EMSS clusters in Donahue *et al.* and several hundred times above that expected for single recombination). The 39 per cent frequency of line emission agrees very well with that found in the EMSS by Donahue *et al.* (1992) in their lower redshift sample. Donahue *et al.* note that the frequency of line emission increases with redshift, which they interpret as an increase in the fraction of cooling flows. This effect is even more remarkable when one notes that the frequency of line emission is higher for clusters with lower luminosity in our sample (46 per cent for clusters with $L_x < 5 \times 10^{44}$ erg s^{-1}, as opposed to 30 per cent for those above that value) and the more distant clusters in the Donahue *et al.* sample are more luminous. Nevertheless, it could also be explained if the fraction of cooling flows with strong line emission increases with redshift. This could be due to a higher incidence of mergers between cooling flows, resulting in more optical line emission. So this sample and the EMSS are consistent in the fraction of emission-line clusters and therefore, by inference, they have a similar fraction of cooling flows.

The radio luminosity may also play an important role in the production of optical line emission (Heckman *et al.* 1989). Edge & Stewart (1991b) show that there is a trend for larger radio powers in larger cooling flows (as noted by Burns 1990), but there are large cooling flows that are not particularly radio luminous, which contradicts the argument of Burns (1990) that the radio sources dominate the energetics of cooling flows. These cooling flows with low radio luminosity also show weak or no line emission (e.g. A478), but there is by no means a direct relationship between low radio and low optical line luminosities, as A2029 contains a moderately radio-luminous cD. At the opposite extreme, the cooling flows with highest radio luminosity (e.g. Cygnus-A and Hydra-A) all show strong optical line emission indicating some link. Clearly, in order to determine the inter-relation of line and radio emission in cooling flows, a detailed X-ray/radio/optical study is required.

4 DISCUSSION

4.1 Which clusters are not cooling flows?

We note that all four of the clusters which are definitely not (focused) cooling flows have two dominant galaxies in their cores (Coma, A2255, A2256 and A3667). From a *ROSAT* observation of A2256 (Briel *et al.* 1991), it is clear that the cluster is merging from the presence of a highly distorted subcluster in the core of the cluster. The X-ray images of the

other three clusters show similar diffuse, elliptical structure so they may all be in the process of merging or have recently merged, supporting the proposal of McGlynn & Fabian (1984) that cooling flows are disrupted when two similarly massive clusters merge. This is also consistent with the observed correlation between the luminosity of the brightest cluster member and the cluster X-ray properties (Edge 1991), where binaries appear to have a brightest galaxy of approximately half the expected luminosity. This implies that the two cluster potentials have already merged and that the two dominant galaxies will eventually merge to form a single galaxy with the expected luminosity. The process of merging will be much slower for systems where the velocity dispersion of the cluster is much larger than that for either of the two dominant galaxies (Tremaine 1990), or for cases where there is a significant amount of angular momentum in the collision. The longer merger time-scale for more massive clusters will result in higher luminosity clusters being more likely to appear as 'binaries'. However, the very highest luminosity clusters are unlikely to be disrupted by a comparable subcluster as the space density of such clusters is so small. This merging scenario would predict a distribution of cooling flows with luminosity having a deficiency at moderate luminosities, as is seen in Table 2. For mergers where the two central galaxies have a large impact parameter and similar masses, they may orbit each other at several hundred kiloparsecs for up to a Hubble time, causing the cooling flow to be well disrupted and spread over the cluster core. Such violent mixing would prevent the quick return of a cooling flow. We also note that A2142 has two dominant galaxies but is a cooling flow, so not *all* mergers disrupt cooling flows.

As an aside, we note that the four non-cooling-flow clusters contain complex radio sources (multiple head–tails and/or radio haloes), A2255 (Harris, Kapahi & Ekers 1980), A2256 (Bridle & Fomalont 1976), Coma (Jaffe, Perola & Valentijn 1976) and A3667 (Goss *et al.* 1982). There are three other putative radio halo sources in the sample, A1367 (Gavazzi & Trinchieri 1983), A2142 (Harris, Bahcall & Strom 1977) and A2319 (Harris & Miley 1978). Five of these clusters are binaries (i.e. have two dominant galaxies) and the other three are either elliptical or have some apparent subcluster in their X-ray structure. Therefore, if binary and/or elliptical clusters are cases of recent mergers, then the radio halo or complex radio emission could arise from the interaction of the intracluster medium (ICM) of each cluster as they collide (Harris *et al.* 1980), as is strongly suggested in A2256 (Fabian & Daines 1991). This would imply that radio haloes are powered by the kinetics of the collision rather than the continuous input of energetic electrons from galaxies or galactic wakes, or that head–tail radio sources are 'triggered' by a merger. Given that a cluster–cluster merger involves two of the most massive, bound objects known ($>10^{14\text{–}15}\ M_\odot$) colliding at velocities above 1000 km s^{-1} (i.e. total kinetic energies of $10^{63\text{–}64}$ erg), it requires only a small acceleration efficiency to inject energetic electrons into the ICM and account for the radio luminosity of these haloes. If this is the case, then roughly the same fraction of clusters should show diffuse radio structures as those showing evidence of mergers in X-rays (roughly 10–20 per cent). The cooling time of the relativistic electrons by the emission of synchrotron radiation of frequency $100\,\nu_8$ MHz in a field of $10^{-6}\ B_{-6}$ G is $\sim 2\times10^9\ \nu_8^{-1/2}\ B_{-6}^{-3/2}$ yr. Consequently, if $B_{-6}>1$ as is inferred for many clusters, the radio halo should be steep at high frequencies, as observed.

One surprise was the observation that the cluster A1367 was found to be on the brink of cooling. A deprojection of the surface brightness profile centred on the diffuse emission (after masking out the two bright point sources) results in a central cooling time very close to the Hubble time. This is unusual as there is no bright galaxy at the cluster centre (all other cooling flows have a galaxy at the X-ray peak). A1367 shows diffuse structure and is thought to be a cluster in the process of forming (Bechtold *et al.* 1983). This apparently 'unfocused' cooling flow has important implications for cooling flow evolution if it is found to be a non-transitory state (i.e. not just after a merger event).

4.2 Implications of evolution and merging

Cooling flows are found in between 70 and 90 per cent of the clusters in the sample, indicating that they are long-lived and common. This high fraction leads to the conclusion that clusters usually have a cooling flow, and only when the cluster merges with another similarly sized cluster is the flow disrupted for a relatively short time. If the 10–30 per cent of clusters which are not cooling are in the process of merging, this allows us to constrain the cluster–cluster merger time-scale to be $2\text{–}4\times10^9$ yr (Edge *et al.* 1990). As pointed out by Richstone, Loeb & Turner (1992), the frequency of mergers and substructure is sensitive to the value of Ω. The short time-scale is consistent with a high-density universe, $\Omega>0.5$.

The observation of strong evolution, coupled with the high frequency of optical and X-ray substructure in clusters, implies that many of the observed properties of clusters, such as radio haloes, are transitory. Some of the kinetic energy in a merger is injected into the cluster core, particularly when the central galaxies merge. This may help power the optical line emission and promote radio activity from the central galaxy. Eventually (in a few billion years) this power is dissipated and the core becomes a quiescent cooling flow with little or no optical line or radio emission. It is unlikely that both the optical and radio emission decline at the same rate, so no simple X-ray/optical/radio correlations can be expected, and none is seen (Section 3.5).

The observed evolution implies that in the future there will be many more massive clusters and hence massive cooling flows ($>1000\ M_\odot$ yr^{-1}). These massive cooling flows will have X-ray luminosities approaching those for the most luminous quasars ($\sim10^{46}$ erg s^{-1}) and a similar space density (10^{-8} Mpc^{-3}).

4.3 Integrated mass flow rate

For any scenario of cluster formation there is a dispersion in the time since collapse for isolated clusters, or the time since the last sizeable merger for most massive clusters. This can be loosely called their 'age'. We must therefore carefully examine how such a range of 'ages' could affect the determination of the mass flow rate in any cooling flow, as it should be closely related to the cluster/cooling-flow 'age', if $\dot{M}\propto r$ and $t_c\propto r^{1.5}$.

We have taken four clusters which have surface brightness profiles with high signal-to-noise ratios, low central cooling times ($<5\times10^9$ yr) and extend to at least 500 kpc, and have

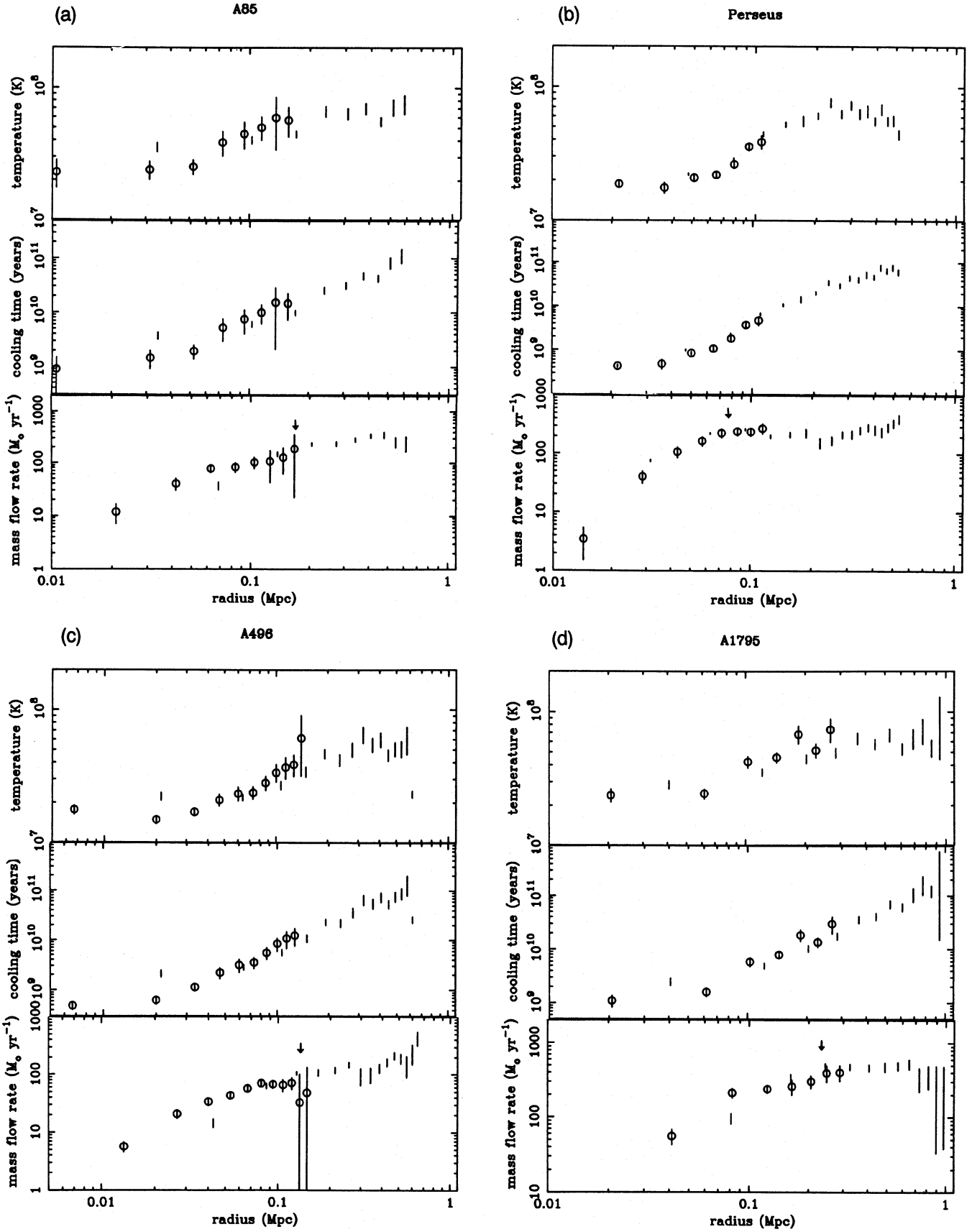

Figure 9. Detailed deprojections for four clusters. The points plotted with circles are HRI data and the others are IPC data. Note that the cumulative mass flow rate refers to the inflow within the complete bin so the data points are plotted at the outer edge of the bin. The temperature and cooling time are determined for the whole bin and are therefore plotted at the centre of each bin. The small arrows indicate the 'breaks' in the $\dot{M}$ profiles.

Table 3. Summary of the detailed deprojections of four clusters with high signal-to-noise ratios. The mass flow rate in brackets is that determined for a critical cooling time of 2×10^{10} yr.

Cluster	'Break' Radius (kpc)	Cooling time (yr)	Mass flow at 'break' ($M_\odot$ yr^{-1})
A85	170–200	$1–2\times10^{10}$	180–230 (236)
Perseus	70 – 100	$2–5\times10^{9}$	240–270 (183)
A496	100–150	$5–10\times10^{9}$	90–110 (112)
A1795	200–230	$1.0–1.5\times10^{10}$	380–470 (478)

studied the mass flow rate profile (Table 3 and Fig. 9). In all cases a 'break' is apparent and the inferred 'ages' are less than or equal to the Hubble time (2×10^{10} yr). A similar feature also appears in the temperature profile. Since the deprojection method requires us to assume the cluster potential, the position and depth of any temperature 'break' is dependent on our assumed potential. However, it is difficult to devise a cluster potential which completely removes any 'break', so we are confident that comparing deprojections of different clusters using the same form of the potential can reveal any relative differences in the mass flow rate and temperature profiles of clusters.

The observed range of ages ($1–1.5\times10^{10}$ yr) is consistent with a 'formation redshift' of 1–2, whereas in the case of the Perseus cluster, the apparent 'age' is less than a quarter of the Hubble time and consistent with a 'formation redshift' of 0.2–0.3. Such apparently young cooling flows are not necessarily formed at these low redshifts but this is when they recovered from their last major merger event. With a larger sample of high-quality images (with spatial resolution of 20–30 kpc to determine the 'break') and matching temperature profiles, it should be possible to calculate the rate of mergers that disrupt cooling flows directly from these 'ages' and hence constrain cluster evolution models. Table 3 shows that the mass flow rates at the 'break' and those for the assumed Hubble time in the analysis (2×10^{10} yr) are similar even when the estimated 'age' of the cluster is much smaller than this. Therefore the assumed value of the Hubble time has little effect on the derived mass flow rates, as long as it is larger than the 'age' of the cluster (i.e. $>1\times10^{10}$ yr).

It should be noted that this 'break' should not be seen as a sharp boundary, since the existence of a multiphase ICM and any cluster asymmetries will tend to blur such features. Therefore it will not be possible to estimate 'ages' with any great accuracy. However,the 'break' is characteristic of the 'mean' phase, so will still reflect the overall 'age' of the flow. Also, it appears that beyond the cooling radius the ICM is remarkably homogeneous and isothermal. This is consistent with high-quality, broad-beam spectra of A478 (Johnstone *et al.* 1992) and Perseus (Allen *et al.* 1992) where only a narrow range of temperature components is found.

To conclude, we emphasize that the flattening of the mass flow rate profile beyond a 'break' radius results in similar total mass flow rates for any assumed critical cooling times above a certain value. This value, the cooling time at the 'break' radius, can be thought of as a cluster 'age' and is always less than 2×10^{10} yr. Hence the mass flow rates given in Table 1 are representative numbers, even though the clusters could have 'ages' differing by as much as a factor of 10 ($2\times10^{9}–2\times10^{10}$ yr) and our assumption of a fixed 'age' is not biasing our results.

5 CONCLUSIONS

From an X-ray flux-limited sample of clusters of galaxies we find a high proportion of cooling flows ($\sim$70 per cent). When we take into account the limited spatial resolution of most of the images used, the proportion rises to 90 per cent, implying that cooling flows are long-lived and common. We show that this result agrees with all other surveys of X-ray clusters and cooling flows when the effects of resolution and selection are taken into account.

The cases where no cooling is found are clusters which are 'binaries', indicating that cooling flows are disrupted during merger activity. This merger activity could also produce the radio structures seen in most of these non-cooling-flow clusters.

In the near future, analysis of the *ROSAT* all-sky survey will provide X-ray images of moderate resolution (1 arcmin) and exposure (400–500 s, equivalent to 1000–1500 s with the IPC). This will allow a similar analysis to be carried out on 200 to 400 clusters, giving a much clearer picture of cooling flows than at the present. When these data are combined with pointed *ROSAT* observations of bright nearby clusters to estimate cooling flow 'ages', and of more distant clusters to determine the fraction of cooling flows at higher redshifts, it will be possible to study the evolution of cooling flows which, if mergers are important, shoud be closely related to the evolution of clusters.

ACKNOWLEDGMENTS

The authors thank Roderick Johnstone, Dave White, Stuart Daines, Keith Arnaud, Richard Mushotzky and Raimund Schwarz for useful comments. ACE and ACF thank the Royal Society for financial support. GCS acknowledges the SERC for support through an Advanced Fellowship.

REFERENCES

Allen, S. W., Fabian, A. C., Johnstone, R. M., Nulsen, P. E. J. & Edge, A. C., 1992. *Mon. Not. R. astr. Soc.*, **254,** 51.
Arnaud, K. A., 1988. In: *Cooling Flows in Galaxies and Clusters*, p. 31, ed. Fabian, A. C., Kluwer Academic Publishers, Dordrecht.
Bechtold, J., Forman, W., Giacconi, R., Jones, C., Schwartz, J., Tucker, W. & Van Speybroeck, L., 1983. *Astrophys. J.*, **265,** 26.
Bridle, A. H. & Fomalont, E. B., 1976. *Astr. Astrophys.*, **52,** 107.
Briel, U. G., Henry, J. P., Schwarz, R. A., Böhringer, H., Ebeling, H., Edge, A. C., Hartner, G. C., Schindler, S., Trümper, J. & Voges, W., 1991. *Astr. Astrophys.*, **246,** L10.
Burns, J. O., 1990. *Astr. J.*, **99,** 14.
Cowie, L. L., Hu, E. M., Jenkins, E. B. & York, D. G., 1983. *Astrophys. J.*, **272,** 29.
Donahue, M., Stocke, J. T. & Gioia, I. M., 1992. *Astrophys. J.*, **385,** 49.
Edge, A. C., 1991. *Mon. Not. R. astr. Soc.*, **250,** 103.
Edge, A. C. & Stewart, G. C., 1991a. *Mon. Not. R. astr. Soc.*, **252,** 414.
Edge, A. C. & Stewart, G. C., 1991b. *Mon. Not. R. astr. Soc.*, **252,** 428.
Edge, A. C., Stewart, G. C., Fabian, A. C. & Arnaud, K. A., 1990. *Mon. Not. R. astr. Soc.*, **245,** 559.

Efstathiou, G., Ellis, R. S. & Peterson, B. A., 1988. *Mon. Not. R. astr. Soc.,* **232,** 431.
Fabian, A. C. & Daines, S. J., 1991. *Mon. Not. R. astr. Soc.,* **252,** 17P.
Fabian, A. C., Nulsen, P. E. J. & Canizares, C. R., 1984. *Nature,* **311,** 733.
Fabian, A. C., Nulsen, P. E. J. & Canizares, C. R., 1991. *Astr. Astrophys. Rev.,* **2,** 191.
Fabian, A. C., Hu, E. M., Cowie, L. L. & Grindlay, J., 1981. *Astrophys. J.,* **248,** 47.
Fabian, A. C., Arnaud, K. A., Nulsen, P. E. J., Watson, M. G., Stewart, G. C., McHardy, I., Smith, A., Elvis, M. & Mushotzky, R. F., 1985. *Mon. Not. R. astr. Soc.,* **216,** 923.
Gavazzi, G. & Trinchieri, G., 1983. *Astrophys. J.,* **270,** 410.
Gioia, I. M., Henry, J. P., Maccacaro, T., Morris, S. L., Stocke, J. T. & Wolter, A., 1990a. *Astrophys. J. Lett.,* **356,** L35.
Gioia, I. M., Maccacaro, T., Schild, R. E., Wolter, A., Stocke, J. T., Morris, S. L. & Henry, J. P., 1990b. *Astrophys. J. Suppl.,* **72,** 567.
Goss, W. M., Ekers, R. D., Skellern, D. J. & Smith, R. M., 1982. *Mon. Not. R. astr. Soc.,* **198,** 259.
Harris, D. E. & Miley, G. K., 1978. *Astr. Astrophys. Suppl.,* **34,** 117.
Harris, D. E., Bahcall, N. A. & Strom, R. G., 1977. *Astr. Astrophys.,* **60,** 27.
Harris, D. E., Kapahi, V. K. & Ekers, R. D., 1980. *Astr. Astrophys. Suppl.,* **39,** 215.
Heckman, T. M., Baum, S., van Breugel, W. J. M. & McCarthy, P., 1989. *Astrophys. J.,* **338,** 48.
Hu, E. M., Cowie, L. L. & Wang, Z., 1985. *Astrophys. J. Suppl.,* **59,** 447.
Jaffe, W., Perola, C. & Valentijn, E., 1976. *Astr. Astrophys.,* **49,** 179.
Johnstone, R. M., Fabian, A. C. & Nulsen, P. E. J., 1987. *Mon. Not. R. astr. Soc.,* **224,** 75.
Johnstone, R. M., Fabian, A. C., Edge, A. C. & Thomas, P. A., 1992. *Mon. Not. R. astr. Soc.,* **255,** 431.
Lahav, O., Edge, A. C., Fabian, A. C. & Putney, A., 1989. *Mon. Not. R. astr. Soc.,* **238,** 881.
McGlynn, T. A. & Fabian, A. C., 1984. *Mon. Not. R. astr. Soc.,* **208,** 709.
Pesce, J. E., Fabian, A. C., Edge, A. C. & Johnstone, R. M., 1990. *Mon. Not. R. astr. Soc.,* **244,** 58.
Richstone, D., Loeb, A. & Turner, E. L., 1992. *Astrophys. J. Lett.,* in press.
Stewart, G. C., Canizares, C. R., Fabian, A. C. & Nulsen, P. E. J., 1984. *Astrophys. J.,* **278,** 536.
Thomas, P. A., Fabian, A. C. & Nulsen, P. E. J., 1987. *Mon. Not. R. astr. Soc.,* **228,** 973.
Tremaine, S. D., 1990. In: *Dynamics and Interactions of Galaxies,* p. 394, ed. Wielen, R., Springer-Verlag, Berlin.
White, D. A., Fabian, A. C., Johnstone, R. M., Mushotzky, R. F. & Arnaud, K. A., 1991. *Mon. Not. R. astr. Soc.,* **252,** 72.
Zabludoff, A. I., Huchra, J. P. & Geller, M. J., 1990. *Astrophys. J. Suppl.,* **74,** 1.